Applied Catalysis B: Environmental 309 (2022) 121239

Contents lists available at ScienceDirect

Applied Catalysis B: Environmental

journal homepage: www.elsevier.com/locate/apcatb

Experimental and in situ DRIFTs studies on confined metallic copper stabilized Pd species for enhanced CO_2 reduction to formate

Xin Xiao [a,b], Jiajian Gao [b], Shibo Xi [b], San Hua Lim [b], Alyssa Kai Wen Png [b,c], Armando Borgna [b], Wei Chu [a,*], Yan Liu [b,*]

[a] School of Chemical Engineering, Sichuan University, No. 24 South Section 1, Yihuan Road, Chengdu 610065, China
[b] Institute of Chemical and Engineering Sciences, A*STAR, 1 Pesek Road, Jurong Island 627833, Singapore
[c] Ngee Ann Polytechnic, 535 Clementi Road, 599489, Singapore

ARTICLE INFO

Keywords:
Enhanced CO_2 hydrogenation to formate
Synergetic effect
PdCu bimetallic catalysts
Confined catalysts
In situ DRIFTs

ABSTRACT

Understanding the basic principle of Pd-based bimetallic catalysts design is essential in CO_2 hydrogenation to formate. In this work, Cu partially replaced the bivalence position in MgAl hydrotalcite structure was developed for achieving the highly confined Cu species, whose interaction with Pd species was systematically studied and compared with the traditional co-impregnation or stepwise impregnation method. The stable and maximum formate formation rate of 12.8 mmol/h/g_{metal} was obtained on $Pd_{0.4}$ @$CuMgAlO_x$ catalyst under 100 °C, 4.0 MPa, H_2/CO_2 ratio of 3, being about double of the sum of formate production rate over the monometallic Cu and Pd catalysts. Strong synergetic interaction between Pd and the confined Cu species was observed with Cu/Pd atomic ratios of 14–181. Extensive characterization using TEM, XPS, XANES, coupled with kinetic study and in situ DRIFTs analysis revealed that the superior performance of $Pd_{0.4}$ @$CuMgAlO_x$ was attributed to the confined PdCu nanoparticles with electron-rich PdCu surface.

1. Introduction

Catalytic reduction of CO_2 into energy vectors and intermediates is of utmost to the energy and environmental requirements [1–3]. Among different endeavors, the selective hydrogenation of CO_2 to formic acid/formate (FA/FM; $HCOOH/HCOO^-$) is a promising approach [4–6]. This is because the target product FA is not only a kind of high-value chemical commonly used for preservative and antibacterial applications [7,8], but renewable energy vectors for hydrogen storage (4.4 wt% hydrogen content) [9,10]. Moreover, compared to other hydrogen carriers like methane or methanol, FA is less flammable, and the stored hydrogen can be easily released through a catalytic dehydrogenation route ($HCOOH \rightarrow H_2 + CO_2$) even at room temperature [11–13].

However, based on the thermodynamic calculation, the hydrogenation of CO_2 to FA is reported to hardly occur in the gas phase ($\Delta G = 33 KJmol^{-1}$), but prone to take place in the aqueous solution (($\Delta G = -4 KJmol^{-1}$) [4,14]. Significant research works have been carried out in this field in recent years [15–17]. The highly active catalysts for CO_2 hydrogenation to FA were mostly found among the homogenous metal complexes, such as Ir, Ru, and Rh-based catalysts [15]. Nevertheless, the homogenous catalysts are limited to industrial plants because of their high cost and tedious separation steps for catalyst recycling [18,19]. Therefore, the development of heterogeneous catalysts is still under a huge requirement. Recently, the supported palladium (Pd)-based heterogeneous catalysts were reported to have superior activity for CO_2 hydrogenation to FA than other noble materials [20–22]. What is more, it was widely accepted that the chemical status, particle size, and the basic sites were the most key factors in CO_2 hydrogenation to FA [18,23,24]. However, from a holistic view on catalysts design, how to integrate all those factors to get catalysts with high performance was still ambiguous. Yan [25] reported that bifunctional sites (basic sites for CO_2 activation and metallic sites for hydrogen dissociation) were necessitated to develop high-performance catalysts in CO_2 hydrogenation to FA. However, basic sites which were critical to generate a high yield of formate on different supports (like ZrO_2 and CeO_2) were varied [25,26]. By engineering the defective of the C_3N_4 sheets, Lee [27] developed acid-treated C_3N_4 with high defective sites supported Pd-based catalysts with benchmark performance in CO_2-to-HCOOH conversion. The interplay between small Pd nanoparticles (~ 3 nm) and the abundant CO_2 supply from nearby defective sits explained this excellent

* Corresponding authors.
E-mail addresses: chuwei1965@scu.edu.cn (W. Chu), liu_yan@ices.a-star.edu.sg (Y. Liu).

https://doi.org/10.1016/j.apcatb.2022.121239
Received 27 November 2021; Received in revised form 16 February 2022; Accepted 21 February 2022
Available online 23 February 2022

performance. Generally, by selecting the appropriate supports, one can easily design the catalysts with basic sites. However, designing metallic Pd sites is more difficult in the development of catalysts with high activity. It was reported that the electronic structure of Pd-based catalysts played an important role in the CO_2 hydrogenation process. Moreover, it can be tuned by the introduction of a second metal. By surface engineering of the PdAg catalysts, Hiromi [28] developed a PdAg catalyst (Pd@Ag/TiO_2) by regulating the surface exposed Pd and Ag atoms. They noticed that the increased catalytic performance over the surface Pd-exposed Pd@Ag catalyst was strongly correlated to the decreased electron density of the active atoms from the synergetic effect of alloying with Ag. However, there are many issues, such as poor chemical stability [29], sintering [30], and low atom-utilization [31] for the noble metallic catalysts, especially when they are used in liquid reactions. One strategy to obtain catalysts with high stability is to keep the nanoparticles in a confined environment.

In particular, layered double hydroxides (LDHs) were widely considered as excellent precursors for developing highly dispersed metallic catalysts with basic sites due to their highly ordered periodic structure and a wide range of host layer elements [32]. The ordered metal oxides grids from the LDHs structure would confine the metal sites and endow the catalysts with high stability in the reaction [3,29]. However, most LDH-derived bimetallic catalysts were reported to be achieved by directly reducing the coprecipitated compounds. The periodic structure of LDH may provide a confined environment but sacrifice the exposed metal surface, which plays a vital role in some reactions. [33] Meanwhile, after thermal treatment, the confined metal usually needs a high temperature for the reduction due to the strong metal-support interaction in the metal oxides. Especially for the Pd-based noble metals, it is easy to aggregate while being reduced at a high temperature. Therefore, designing stale Pd-based catalysts from LDHs derived materials for CO_2 hydrogenation to FM remains a challenge. Meanwhile, the basic principles and fundamental understanding of the LDHs derived bimetallic catalysts still need further investigation. This work presented a novel Pd-based bimetallic catalyst stabilized by the surface confined Cu species derived from the LDHs materials, aiming to improve CO_2 hydrogenation to FM. Compared to the reported IB group Ag or Au-based catalyst, element Cu located in the same IIB group was selected here because it was cheaper and easier to be incorporated into the layer structure, which would lead Cu highly dispersed and confined stably in the oxides grid. To achieve catalysts with low cost and high performance, the PdCu catalysts with low Pd/Cu atomic ratios were synthesized by introducing Pd onto the MgAlOx confined highly dispersed Cu species. Extensive characterizations (XRD, TEM, XPS, XANES, etc.) and in situ DRIFTs were carried out to understand the rational principle towards a high-performance PdCu catalyst in CO_2 hydrogenation to formic acid. The results indicated that a well-observed synergetic effects between Pd and the confined Cu species over $Pd_{0.4}$ @CuMgAlOx catalysts at Cu/Pd = 42 (molar ratio). It exhibited the excellent catalytic activity and durability with a high turnover number (TON, based on Pd) of 1511 for a 24-hour reaction at 100 °C under a total pressure of 40 bar.

2. Experimental

2.1. Preparation of CuMgAl-LDH, MgAl-LDH, and derived mixed oxides

CuMgAl-LDH and MgAl-LDH were prepared by a modified co-precipitation as the literature reported [3,29]. To obtain CuMgAl-LDH, 1.21 g copper (II) nitrate hydrate, 10.24 g magnesium nitrate hexahydrate, and 3.75 g aluminum nitrate nonahydrate were first dissolved together in 100 mL de-ionized (DI) water. This solution was referred as solution A. Solution B consists of 100 mL of sodium carbonate solution (0.15 M). To get the LDH precursors, solution A was added dropwise into solution B under vigorous stirring at 65 °C. During this process, 1.0 M sodium hydroxide solution (solution C) was added to maintain the solution pH value of 10. After co-precipitation, the slurry was aged at 65 °C for 5 h, filtered off, and washed with DI water until pH reached 7. The precipitate was then dried at 100 °C overnight and marked as CuMgAl-LDH. Sample MgAl-LDH was prepared using a similar method and Mg/Al was kept at 4.0 as that in CuMgAl-LDH. Mixed oxides were derived from four-hour calcination of obtained CuMgAl-LDH and MgAl-LDH precursors at 500 °C in static air. They were labeled as CuMgAlOx and MgAlOx, respectively.

2.2. Preparation of different Pdx@CuMgAlOx

Pdx@CuMgAlOx samples with different Pd loadings were prepared by the impregnation-reduction method. To prepare $Pd_{0.4}$ @CuMgAlOx, 1 g of prepared CuMgAlOx was added into 20 mL DI water containing 1.03 mL of $PdCl_2$ solution (0.023 M). After 2-hour stirring at room temperature, the water was subsequently removed via rotary evaporation and the obtained solid was then dried in 100 °C oven overnight. $Pd_{0.4}$ @CuMgAlOx was obtained by further in-situ reduction of the dried sample at 550 °C by 50 sccm of 5% H_2/Ar mixed gas for 1 h. Other Pdx@CuMgAlOx samples were prepared using the same procedure but with different volumes (4.0 mL, 2.0 mL, 0.6 mL, 0.3 mL) of $PdCl_2$ solution (0.023 M), being identified as $Pd_{1.3}$ @CuMgAlOx, $Pd_{0.6}$ @CuMgAlOx, $Pd_{0.2}$ @CuMgAlOx and $Pd_{0.1}$ @CuMgAlOx, respectively.

2.3. Preparation of Pd0.4-Cu/MgAlOx, Cu-Pd0.4/MgAlOx, Pd0.4Cu/MgAlOx-IM catalysts

$Pd_{0.4}$-Cu/MgAlOx was prepared by impregnation-reduction of Pd over CuO/MgAlOx. Typically, for $Pd_{0.4}$-Cu/MgAlOx, CuOx/MgAlOx was first prepared by impregnation. Typically, 0.42 g copper (II) nitrate hydrate was dissolved in 20 mL of DI water. 1 g MgAlOx was then added into the dissolved solution, which formed a slurry. After stirring at room temperature for 2 h, water in the slurry was eliminated via rotary evaporation and the obtained solid was dried overnight in the oven at 100 °C. CuOx/MgAlOx was obtained by thermal treatment of the dried sample at 500 °C for 4 h under static air. $Pd_{0.4}$-Cu/MgAlOx was prepared similarly as $Pd_{0.4}$ @CuMgAlOx, but the CuMgAlOx support was substituted by CuOx/MgAlOx.

Cu-$Pd_{0.4}$/MgAlOx was prepared by sequential impregnation-reduction of Pd and Cu supported on MgAlOx. 1 g MgAlOx was added into 20 mL of DI water containing 1.03 mL of $PdCl_2$ (0.023 M). After stirring at room temperature for 2 h, the solvent was removed via rotary evaporation and the solid was dried overnight in the oven at 100 °C, referred as $PdCl_2$/MgAlOx. Subsequently, the dried $PdCl_2$/MgAlOx was added into 20 mL of DI water with 0.42 g copper (II) nitrate hydrate and kept stirring at room temperature for 2 h. The solvent was removed via rotary evaporation. Cu-Pd/MgAlOx was prepared with a similar in-situ reduction method as that on $Pd_{1.03}$ @CuMgAlOx after drying.

$Pd_{0.4}$Cu/MgAlOx was prepared by co-impregnation and sequential reduction method. Similar to that on $Pd_{0.4}$ @CuMgAlOx, the precursors of $Pd_{0.4}$Cu/MgAlOx were obtained after drying overnight. The precursors of Pd and Cu in $Pd_{0.4}$Cu/MgAlOx were fixed as the same as that in $Pd_{0.4}$-Cu/MgAlOx. $Pd_{0.4}$Cu/MgAlOx samples were obtained by in-situ reduction of dried precursors at 550 °C using 50 sccm of 5% H_2/Ar mixed gas for 1 h.

2.4. Characterization of catalysts

Powder X-ray diffraction (XRD) patterns of the prepared CuMgAl-LDH, CuMgAlOx, and reduced PdCu catalysts were collected on a powder diffraction-meter (Bruker D8 Advance X-ray) with a Cu-Kα resource (Kα= 0.154 nm) within the 2θ range of 5° to 85°. Elemental analysis was conducted on an Agilent VISTA-MPX inductively coupled plasma-optical emission spectroscopy (ICP-OES). X-ray photoelectron spectroscopy (XPS) was collected using an XSAM800 XPS equipped with an Mg-Kα source. The obtained XPS patterns were calibrated with the

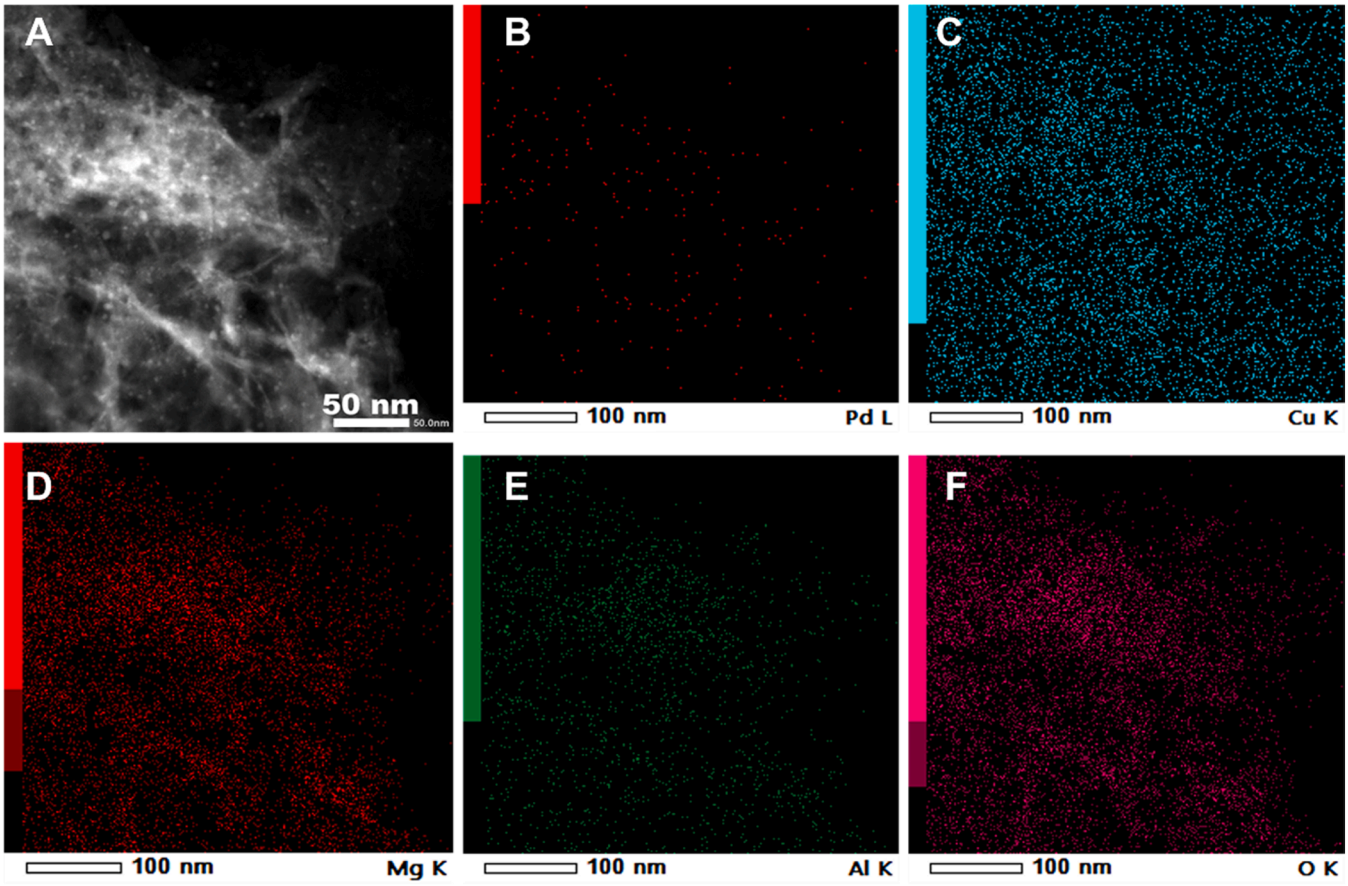

Fig. 1. Dark-field TEM images of $Pd_{0.4}$ @CuMgAlOx catalysts (A) and EDX mapping image of different elements (B–F).

C1s peak at 284.6 eV. The specific surface areas of different PdCu catalysts were measured by the low-temperature (−196 °C) N_2 adsorption/desorption isotherms. Before the test, the samples after 5% H_2/Ar treatment were degassed at 200 °C for 24 h. The specific surface area was determined by the Brunauer-Emmett-Teller (BET) equation and the pore-size distribution was obtained from the desorption branch with Barrett-Joyner-Halenda(BJH) method. The CO-chemisorption test was carried on the Micromerities Autochem 2920. Typically, 50 mg of 550 °C pre-reduced $Pd_{0.4}$ @CuMgAlOx sample was placed in a U-shape quartz tube, which was slowly ramped to 100 °C in He for 1 h, and reduced in 10% H_2/Ar mixture at 400 °C for 1 h and then cooled down to 25 °C under the flow of He. Thereafter, pulse chemisorption with 10% CO/He until the TCD signal reached a constant value for collecting the total CO uptake. The number of exposed palladium atoms on the surface was calculated based on the amount of the chemisorbed CO in the reported methods. [34] The morphology of the prepared Cu-containing precursor was examined using field emission scanning electron microscopy (FESEM, JSM-6700 F). Transmission electron microscopy (TEM) experiments were carried on the JEM-2010 with energy dispersive X-ray spectroscopy (HRTEM/EDX, JEM-2100 F, 200 kV). The PdCu catalysts were reduced at 550 °C for 1 h before TEM characterization. The X-ray absorption near edge structure (XANES) and the extended X-ray absorption fine structure (EXAFS) tests of Pd K-edge and Cu K-edge of the $Pd_{0.4}$Cu samples were measured at the XAFCA beamline of Singapore Synchrotron Light Source (SSLS) [35]. The storage ring of SSLS operated at E = 700 MeV and Imax = 200 mA. The radiation was monochromatized by the Si(111) double-crystal monochromator. Pd powder and Cu foil were taken as references for energy calibration. *In situ* DRIFT data were collected on a PerkinElmer FTIR spectrophotometer using an in situ cell, which allowed the treatments under different gases. Firstly, the 550 °C pre-reduced catalysts (50 mg) were activated in pure He flow (30 mL/min) at 100 °C for 30 min. After taking the background spectrum under the flowing He atmosphere at 100 °C, the gas flow was switched into a mixture gas of CO_2/H_2 (3/1, 50 mL/min). The DRIFTs spectra were continuously recorded from 40 s up to 30 min at 3 min interval, at 100 °C.

2.5. Catalytic performance test

Before each test, 100 mg catalysts were reduced by 50 mL/min of 5% H_2-Ar mixed gas for 1 h at 550 °C. The catalytic performance tests were carried out in a 100-mL Parr reactor with a glass vial. In a typical test, 10 bar of CO_2 and 30 bar of H_2 were compressed in the reactor after adding 30 mL of 1.5 M NaOH into the glass inlet and purging with CO_2 to remove the air from the reactor system. A stirring speed of 400 rpm and a temperature of 100 °C were controlled during the reaction processing. After completing the reaction, the liquid phase of the reaction mixture was collected by centrifugation at 6000 rpm for 4 min. Then 2 μL of the liquid was taken to determine the generated amount of formate. The yield of formate was determined by an HPLC (Shimazu-2013) equipped with a Bio-Rad Aminex HPX-87 Ion Exclusion Column (300 mm × 7.8 mm). 5 mM H_2SO_4 (0.600 mL/min) was used as a mobile phase.

3. Results and discussion

3.1. Preparation and characterization of PdCu catalysts

To achieve the confined highly dispersed Cu species, the ternary CuMgAl-LDH was synthesized via the partial replacement of Cu in the bivalence position in the MgAl hydrotalcite structure. Fig. S1 (Supporting Information) showed the XRD patterns of the obtained LDH

Table 1
Catalytic performance of Pd(Cu) catalysts for CO_2 hydrogenation to formate.

Entry	Samples[a]	Yield of formate (mmol)	Formate formation rate[b] (× 10^3 umol/g $_{(Pd+Cu)/h}$
1	CuMgAlOx	0.51	1.93
2	$Pd_{0.1}$ @CuMgAlOx	0.96	3.61
3	$Pd_{0.2}$ @CuMgAlOx	1.19	4.45
4	$Pd_{0.4}$ @CuMgAlOx	3.49	12.8
5	$Pd_{0.6}$ @CuMgAlOx	2.23	8.06
6	$Pd_{1.3}$ @CuMgAlOx	0.44	1.49
7	$Pd_{0.4}$/MgAlOx	1.25	4.57

[a] Reaction conditions: catalyst (100 mg), 1.5 M NaOH solution (30 mL), H_2/CO_2 (3:1, total pressure 40 bar (room temperature), 100 °C, 24 h.
[b] Formate formation rate was calculated based on per gram of Pd and Cu per hour.

precursor. The pronounced diffraction peaks at around 11.4°, 22.8°, 34.6°, 45.2°, 60.5°, and 61.8° were indexed to the (003), (006), (012), (015), (018), (110), and (113) reflections of hydrotalcite (JCPDS 22-0700), respectively [36]. This result suggested the successful incorporation of copper into the MgAl-hydrotalcite regardless of the Jahn-Teller effect [37]. The observed hexagonal nanosheet in the SEM image (Fig. S2A, Supporting Information) confirmed the obtained layer structure and indicated the formation of ternary hydrotalcite. Further investigation of XRD patterns over the reduced Pd-Cu bimetallic catalysts was presented in Fig. S2B (Supporting Information). Two distinct diffraction peaks at about 43.2° and 63.5° were observed on all the reduced samples. The peak at 63.5° was assigned to the diffraction of MgO [38], which accounts for ~ 70 wt% of the catalysts. Interestingly, no distinct peaks ascribed to the metallic copper or palladium were observed. It might imply the small size of Pd/Cu species after 550 °C reduction. Fig. S3 (Supporting Information) showed the N_2 adsorption-desorption isotherms of the reduced samples. The type IV isotherms curve and H_3-type hysteresis loops in all the samples were observed on all the samples, indicating the presence of mesoporous structure [39,40]. The tabulated textural properties in Table S1 (Supporting Information) showed a similar surface area and pore size distribution regardless of the loading amount of Pd, and the main surface area was originated from the support MgAlOx and CuMgAlOx. These results confirmed the unchangeable structure by loading of Pd. Meanwhile, the TEM-EDX analysis showed the uniformly distributed Pd and Cu over $Pd_{0.4}$ @CuMgAlOx (Fig. 1B–F) catalysts. The presence of the layered structure was further observed in the dark-field TEM images in Fig. 1A. The structure was well maintained with the highly dispersed ultrafine metallic PdCu particles (~ 3.5 nm) even after thermal reduction at 550 °C H_2/Ar mixed gas, indicating the thermal resistance of the hydrotalcite-derived mixed oxides.

Figs. S4 and S5 (Supporting Information) displayed the dark-field TEM-EDX images comparison of the reduced CuMgAlOx and bimetallic $Pd_{0.4}$ @CuMgAlOx using a nickel TEM grid. Fig. S4 presented the uniformly dispersed copper in the mixed oxides before forming PdCu bimetallic catalyst. The bright dot zone (zone I in Fig. S4D) presented a clear outline like the distribution of Mg, Al, O elements in the sample CuMgAlOx. These results further proved that the copper was well dispersed in the hydrotalcite structure before becoming bimetallic catalysts, which may originate from the periodic structure of CuMgAl-LDH precursor. Fig. S5 displayed the dark-field TEM-EDX images of the reduced bimetallic $Pd_{0.4}$ @CuMgAlOx. The tiny bright dots in Fig. S5A demonstrated a small particle size distribution of the PdCu bimetallic catalyst. The distinct outline of copper in the bright zone (Zone O) of Fig. S5D and the uniformly dispersed Pd in Fig. S5E proved the well-dispersion of Cu and Pd after reduction. Moreover, the EDS spot scan

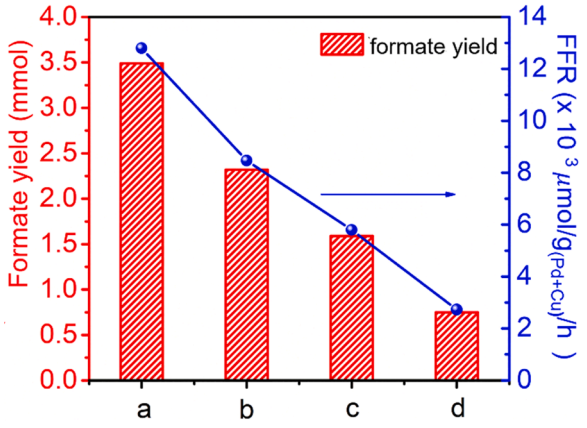

Fig. 2. Catalytic performance of $Pd_{0.4}Cu$ bimetallic catalysts prepared via different methods. a: $Pd_{0.4}$ @CuMgAlOx, b: $Pd_{0.4}Cu$/MgAlOx, c: $Pd_{0.4}$-Cu/MgAlOx, d: Cu-$Pd_{0.4}$/MgAlOx. FFR: formate formation rate. Reaction condition: 100 mg catalysts, 30 mL 1.5 M NaOH, 40 bar (room temperature) of CO_2 and H_2 mixture gas (CO_2/H_2 = 1:3), 100 °C, 24 h.

in Fig. S6 (Supporting Information) indicated the Pd, Cu component in the observed bright dots, confirming the formation of PdCu bimetallic catalysts. Results suggested the anti-Ostwald ripening properties [41] and confirmed the uniform nano PdCu particles in the hydrotalcite derived structure.

3.2. Catalytic performance of PdCu catalysts

The performance of CO_2 hydrogenation was tested in a 100 mL Parr reactor with the medium of 1.5 M NaOH (30 mL). As summarized in Table 1, the catalytic performance over monometallic copper was initially investigated. 0.51 mmol of formate was obtained over the catalyst CuMgAlOx (entry 1). As no activity of Cu-N @ MHCS was observed in the previous report [42], our results indicated that metallic Cu in the LDH derived structure might play a vital role in CO_2 hydrogenation to formate. After introducing Pd, the formate yield increased to 0.96 mmol (entry 2), suggesting the Pd-promote hydrogenation process in this reaction. Generally, the catalytic activity would greatly depend on the composition of the bimetallic catalyst [43–45]. To find the optimal content of Pd and Cu, the effect of Pd loading was studied. The yield of formate displayed as a volcano-shaped curve with the loading of Pd increasing on Pdx@CuMgAlOx series catalysts (entries 2–7). Sample $Pd_{0.4}$ @CuMgAlOx (entry 4) showed the best catalytic performance among all the PdCu bimetallic catalysts. Specifically, the formate yield on $Pd_{0.4}$ @CuMgAlOx was 3.49 mmol, being 6.8 times as that over CuMgAlOx and 2.8 times as that over monometallic Pd (entry 7). By the characterization of ICP-OES on $Pd_{0.4}$ @CuMgAlOx (Table S1, Supporting Information), the loading of Pd and Cu was 0.4 wt% and 10.8 wt%, respectively. It indicates a high mole ratio of Cu to Pd (45:1), far different from the 2:7 of PdCu molar ratio in the reported PdCu@N-MHCS [42]. To further understand the catalytic performance of PdCu catalysts and the contribution of Pd, the formate formation rate normalized by the metal mass (both Pd and Cu) in the catalyst was calculated (last column in Table 2). The formate formation rate (FFR) showed a similar trend as the yield of formate over the PdCu catalysts. For instance, $Pd_{0.4}$ @CuMgAlOx showed a superior FFR among PdCu catalysts, which was about two times higher than the sum of those over monometallic Cu and Pd catalysts. The results suggested that both the metallic Pd and Cu played a vital role in the formate formation, and the synergetic effect of Pd and Cu endowed the superior catalytic performance of $Pd_{0.4}$ @CuMgAlOx catalyst in this work.

Additionally, to adopt the appropriate preparation method for PdCu catalysts, PdCu bimetallic catalysts with the same loadings of Pd and Cu in $Pd_{0.4}$ @CuMgAlOx were prepared by co-impregnation and stepwise

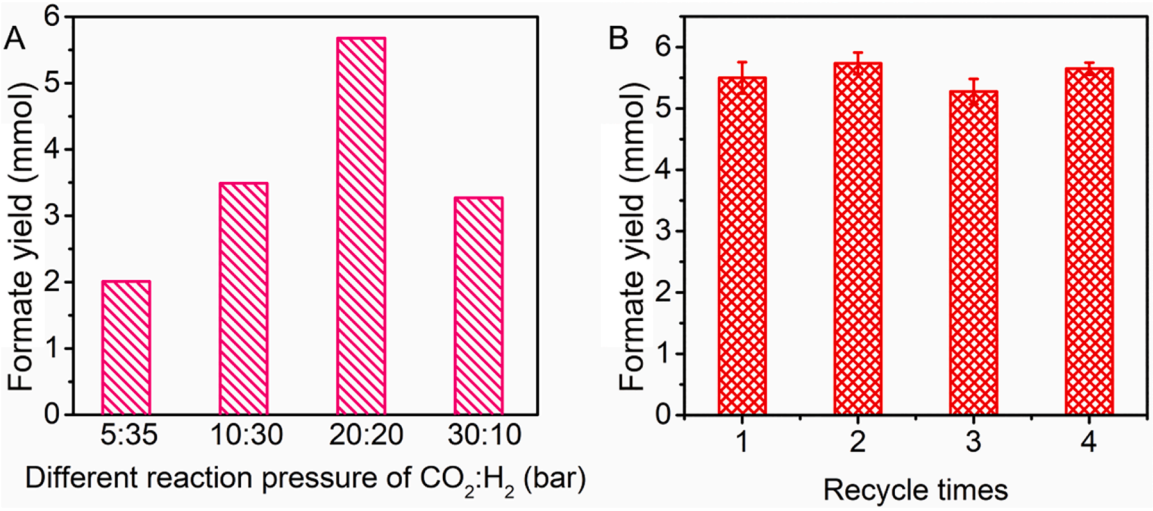

Fig. 3. (A) Catalytic performance of $Pd_{0.4}$ @CuMgAlOx catalyst under 40 bar with different CO_2/H_2 test conditions. Reaction condition: 100 mg catalysts, 30 mL 1.5 M NaOH, 40 bar (room temperature) of CO_2 and H_2 mixture gas, 100 °C, 24 h. (B) recycle test of $Pd_{0.4}$ @CuMgAlOx catalyst. Reaction condition: 100 mg catalysts, 30 mL 1.5 M NaOH, 40 bar (room temperature) of CO_2 and H_2 mixture gas ($CO_2/H_2 = 1$), 100 °C, 24 h.

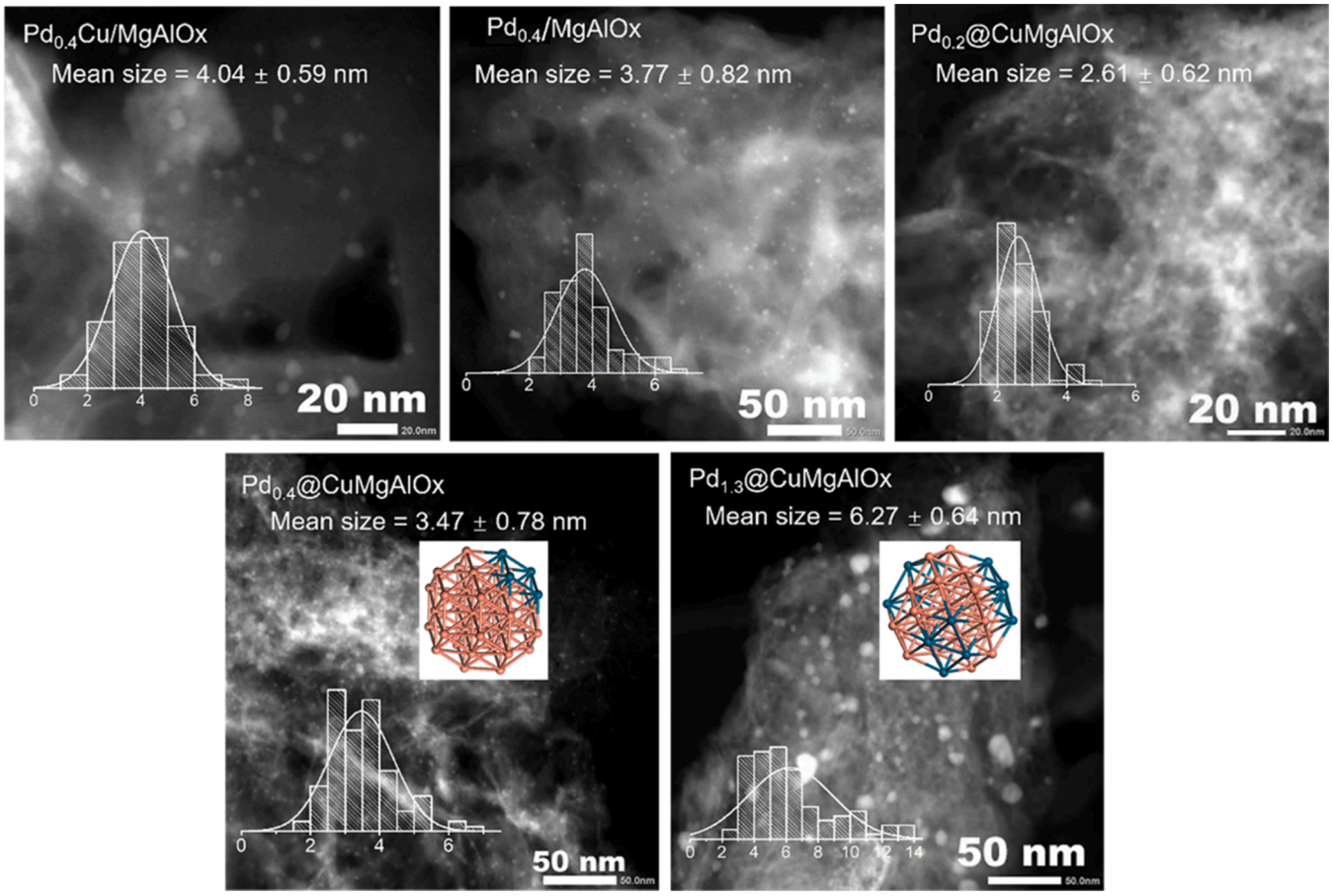

Fig. 4. Dark-field TEM images of typical Pd and PdCu catalysts together with the particle size distribution.

impregnation methods. Fig. 2 plots the formate yield and formate formation rate over PdCu catalysts versus the different preparation methods. The Cu-$Pd_{0.4}$/MgAlOx prepared via stepwise impregnation (Pd followed by Cu) gave the lowest value among those catalysts. The formate yield decreases as $Pd_{0.4}$ @CuMgAlOx > $Pd_{0.4}$Cu/MgAlOx (PdCu co-impregnation) > $Pd_{0.4}$-Cu/MgAlOx (Cu followed by Pd) > Cu-$Pd_{0.4}$/MgAlOx. Results suggested that: (i) catalysts derived from confined metal oxides were superior to those prepared by the impregnation methods; (ii) the catalytic performance was sensitive to the impregnation sequence of metal precursors. For instance, the formate yield on $Pd_{0.4}$ @CuMgAlOx is 1.5 times of that on $Pd_{0.4}$-Cu/MgAlOx, while the formate yield on $Pd_{0.4}$-Cu/MgAlOx (1.59 mmol) was more than 2 times as that on Cu-$Pd_{0.4}$/MgAl (0.75 mmol), further indicating the importance of preparation methods of PdCu bimetallic catalysts.

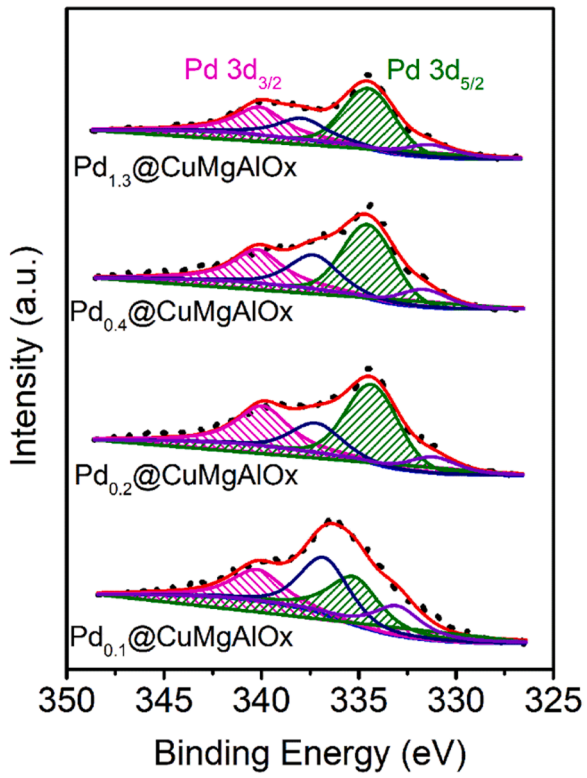

Fig. 5. XPS spectra of Pd 3d (Mg Kα source) over typically confined PdCu catalysts.

Fig. 3A showed the effect of the CO_2/H_2 ratio on the formate yield over the optimal $Pd_{0.4}$ @CuMgAlOx catalyst. Under a total pressure of 40 bar, the highest formate yield (5.68 mmol, TOF: 411 h^{-1}, based on Pd, from CO chemisorption analysis) was achieved at the 20/20 (bar) of CO2/H2. As shown in the Table S3 (Supporting Information), the sample $Pd_{0.4}$ @CuMgAlOx displayed a comparable performance in the reported Pd-IB bimetallic catalyst. A high TON value of 9864 (based on the surface amount of Pd obtained from CO chemisorption analysis) was reached. Considering the low-cost of copper, the catalyst of $Pd_{0.4}$ @CuMgAlOx demonstrated relatively high advantages for industrial applications. Further stability tests were carried by the multiple catalyst recycling experiments under typical reaction conditions with $CO_2/H_2 = 1$. As shown in Fig. 3B, the $Pd_{0.4}$ @CuMgAlOx showed no significant loss in formate yield after the fourth run, indicating its good stability.

3.3. Understanding the key parameters in CO_2 hydrogenation to formate over confined PdCu bimetallic catalysts

Fig. 4 displayed the TEM analysis on the typical Pd and PdCu catalysts prepared with different Pd loadings and using co-impregnation method. It was found that most of those catalysts had a small Pd or PdCu particle size of 2–4.5 nm, except the large particle size (6.27 nm) was observed on the sample $Pd_{1.3}$ @CuMgAlOx with high Pd loading (1.3 wt%). Specifically, the particle size of the $Pd_{0.4}$ @CuMgAlOx prepared via confined Cu species in MgAl layered structure was smaller (3.47 nm) than that prepared by the conventional preparation method ($Pd_{0.4}$Cu/MgAlOx, 3.77 nm). Correlating to the activity data presented in Table 2, it can be concluded that the formate formation rate over PdCu bimetallic catalyst was sensitive to the PdCu particle size, being consistent to what reported in literature.[46] The optimal particle size (3.4 nm) was achieved on $Pd_{0.4}$ @CuMgAlOx, similar to the reported 0.6 Pd@g-C_3N_4 (3.38 nm) [47]. Meanwhile, larger particle size may undermine the catalytic performance due to its aggregation of PdCu nanoparticles.

Fig. 5 showed the XPS spectra of Pd 3d on the typical PdCu bimetallic catalysts. Two peaks were observed at ~334 and 340 eV corresponding to the Pd (0) in Pd $3d_{5/2}$ and Pd $3d_{3/2}$ [48], while other peaks at ~332 eV and ~ 337 eV might be ascribed to the shoulder peak of the Cu LMM Auger spectra [49] and the Cu LMM Auger spectra of Cu metal [50], respectively. In particular, compared to the reported metallic Pd $3d_{5/2}$ (~ 335 eV) [48,51], the $Pd_{0.1}$ @CuMgAlOx catalyst showed a 0.2 eV positive shift in the binding energy of Pd $3d_{5/2}$. This result may originate from the low surface ratio of Pd/Cu (molar ratio 0.006). In this case, the catalyst enriched with Cu and the spectra would be impacted mainly by the Cu LMM Auger spectra. With the increase of Pd loading, more and more Pd-Cu bonds formed in samples with 0.2–1.3 wt% of Pd. Due to the different ionization potentials of Pd and Cu (Pd: 8.34 eV, Cu:7.73 eV), the electron would transfer from the confined Cu to Pd. Therefore, as shown in Fig. 5, the binding energy of Pd $3d_{5/2}$ in those 0.2–1.3 wt% of Pd-based samples shifted to lower energy (0.6–0.7 eV) than that of the reported metallic Pd.

As aforementioned in Fig. 2, the catalytic performance over PdCu catalysts was also sensitive to the incorporation methods. To understand the advantage of our preparation method via confined Cu species in MgAl-LDH derived structure ($Pd_{0.4}$ @CuMgAlOx catalyst) at an atomic level, the XANES at the Pd L_{III}-edge and Cu K-edges were collected (Figs. 6 and 7). As shown in Fig. 6A, compared with the co-impregnation and stepwise impregnation method, the white line energy of L_{III}-edge for Pd in $Pd_{0.4}$ @CuMgAlOx was the lowest, suggesting the relatively most electron rich status of Pd, followed by $Pd_{0.4}$Cu/MgAlOx, and $Pd_{0.4}$-Cu/

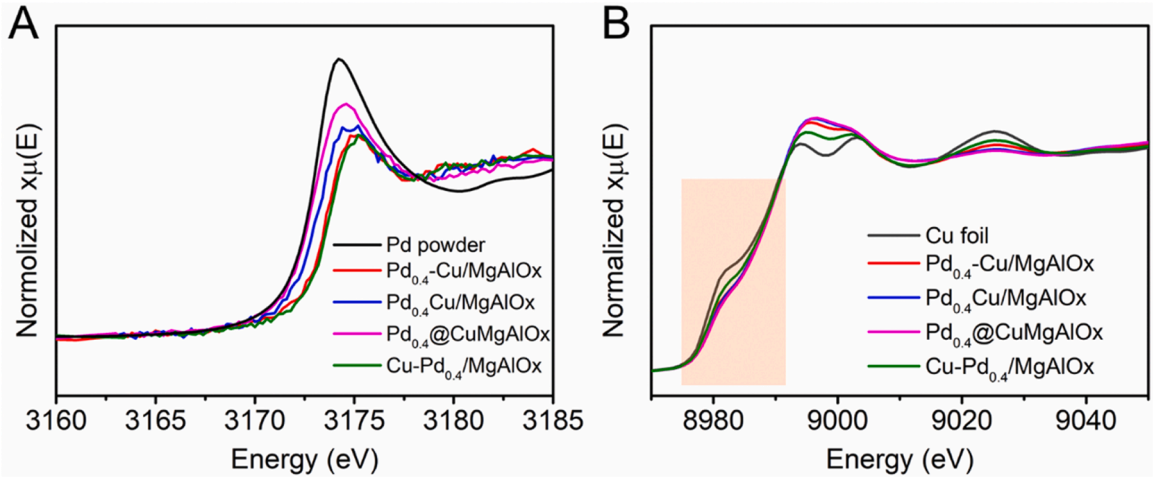

Fig. 6. Pd L_{III}-edge (A) and Cu K-edge (B) XANES of the Pd powder, $Pd_{0.4}$-Cu/MgAlOx, $Pd_{0.4}$Cu/MgAlOx, $Pd_{0.4}$ @CuMgAlOx, and Cu-$Pd_{0.4}$/MgAlOx samples.

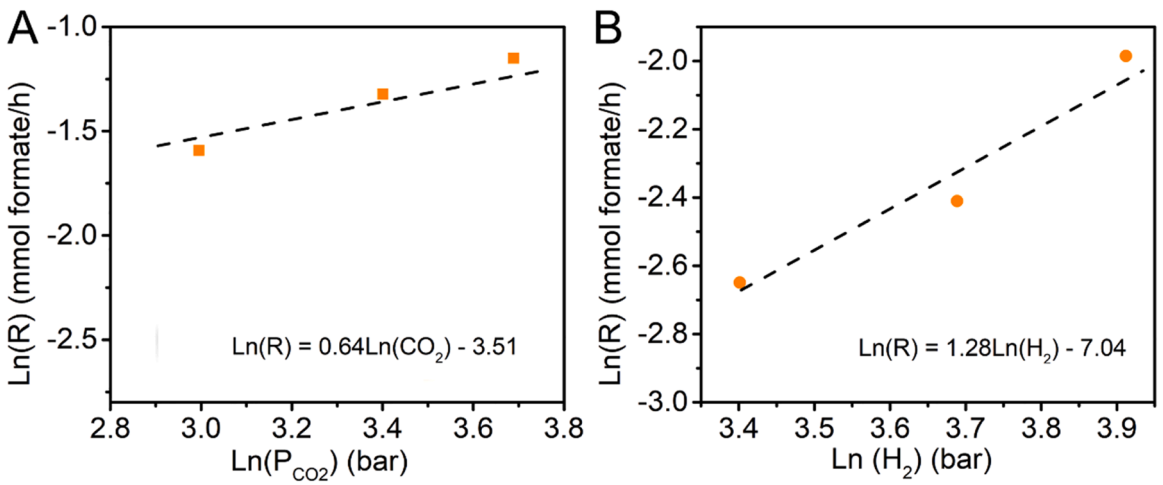

Fig. 7. (A) Logarithm plots of formate yield rate and the partial pressure of CO_2 (P_{CO2}) in the CO_2 hydrogenation and (B) logarithm plots of formate yield rate and the partial pressure of H_2 (P_{H2}) in the CO_2 hydrogenation.

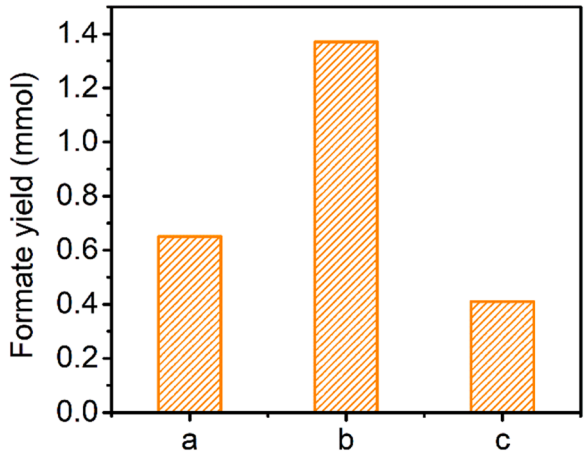

Fig. 8. Catalytic performance of $NaHCO_3$ hydrogenation over typical PdCu catalysts. a: $Pd_{0.2}$ @CuMgAlOx, b: $Pd_{0.4}$ @CuMgAlOx, c: $Pd_{1.3}$ @CuMgAlOx. Reaction condition: 100 mg catalyst, 30 mL of 1.5 M $NaHCO_3$, H_2 (40 bar), 100 °C, 24 h.

MgAlOx, Cu-$Pd_{0.4}$/MgAlOx, which supposed to be the crucial factor for the formate formation rate as shown in Fig. 2. Meanwhile, as shown in Fig. 6B, the Cu K-edge XANES spectra for $Pd_{0.4}$ @CuMgAlOx was most different to that of the Cu foil. The lowest intensity of Cu in $Pd_{0.4}$ @CuMgAlOx at the shoulder peak zone (8975 ~ 8985 eV) indicated its most electron-deficient status. The FT-EXAFS (Fig. S7, Supporting Information) of the Cu K-edge showed that all samples exhibited a pronounced peak for Cu-Cu bond coordination at 2.2 Å. The lowest intensity of sample $Pd_{0.4}$ @CuMgAlOx in Fig. S7 further suggested a smaller particle size or higher degree of disorder in this sample. Combining with the Pd L_{III}-edge spectra, it can be found out that the electron was transferred from Cu to Pd and resulted in the electron-rich Pd ($Pd^{\delta-}$) and electron-deficient Cu ($Cu^{\delta+}$) species. As reported in the literature [28], the bimetallic catalysts with electron-rich Pd would enhance the catalytic performance in CO_2 hydrogenation. Our $Pd_{0.4}$ @CuMgAlOx catalyst prepared via the confined Cu species via MgAl-LDH derived method indeed gave the highest formate yield due to their most electron-rich of Pd active species in the catalyst.

To determine the critical factors for the conversion of CO_2 to formate, the reaction kinetics was analyzed. The reaction rate (R) of the CO_2 hydrogenation reaction can be presented as $R = kP_{CO2}^{\alpha}P_{H2}^{\beta}$ [52], where k represents the rate constant, P_{CO2} and P_{H2} are the partial pressures of CO_2 and H_2. α and β are the reaction order of CO_2 and H_2, respectively. Here, the parameter α and β for $Pd_{0.4}$ @CuMgAlOx catalyst were obtained as 0.64 and 1.28 at 100 °C, by conducting the reaction under different CO_2 and H_2 pressure. The higher value of β indicated that the CO_2 hydrogenation rate was more dependent on the H_2 pressure. The formate yield rate could be significantly enhanced by increasing the partial pressure of H_2. Generally, when using a base solution (like NaOH, KOH) for CO_2 hydrogenation, the injected gaseous CO_2 was reported to form bicarbonate (HCO_3^-) with the reaction base intermediates. The formed bicarbonate would be further hydrogenated to form formate [21, 53]. During this process, the Pd-based metallic sites governed the H_2 dissociation by forming the active Pd-hydride and further determining the hydrogenation rate of the formed bicarbonate [53]. Therefore, the hydrogenation of $NaHCO_3$ experiments was conducted over the typical PdCu catalysts to verify this hypothesis.

As displayed in Fig. 8, the formate yield decreased as follows: $Pd_{0.4}$ @MgAlOx > $Pd_{0.2}$ @CuMgAlOx > $Pd_{1.3}$ @CuMgAlOx for the hydrogenation of $NaHCO_3$. Notably, the formate yield shared the same trend as that used gaseous CO_2 as the reactant, indicating that $NaHCO_3$ acted as a critical reaction intermediate [54]. However, compared to the experiments using CO_2 as the carbon sources (Table 1), the formate yield was far lower in the bicarbonate hydrogenation reactions. It may be ascribed to the different pH values in the sodium hydroxide and bicarbonate solution. It was reported that the base solution with high basicity would promote CO_2 absorption and enhance the formate yield for CO_2 hydrogenation [52], which was similar to those were reported on PdAg catalysts [53].

3.4. *In situ experiment study on the confined PdCu catalysts*

To further study the behavior of the CO_2 hydrogenation reaction over the confined PdCu catalysts, the in situ DRIFT experiments were conducted over the typical monometallic catalysts ($Pd_{0.4}$/MgAlOx, CuMgAlOx), the optimal $Pd_{0.4}$ @CuMgAlOx and $Pd_{1.3}$ @CuMgAlOx catalysts. Fig. 9 showed the collected DRIFT spectra under the atmosphere of CO_2 and H_2 at 100 °C. Similar vibrational features were observed, mainly including bidentate carbonate (labeled in red numbers), monodentate carbonate(labeled in blue numbers), bicarbonate (labeled in green numbers), formate species (labeled in orange numbers), and unassigned carbonate (labeled in purple and black numbers) [55–57]. However, their intensity and evolution were quite different. On CuMgAlOx, bidentate carbonate was the primary surface species. While over the Pd-containing catalysts ($Pd_{0.4}$/MgAlOx, $Pd_{0.4}$ @CuMgAlOx, and $Pd_{1.3}$ @CuMgAlOx), the intensity of the absorbed bidentate carbonate species sharply decreased and the most abundant species turned into

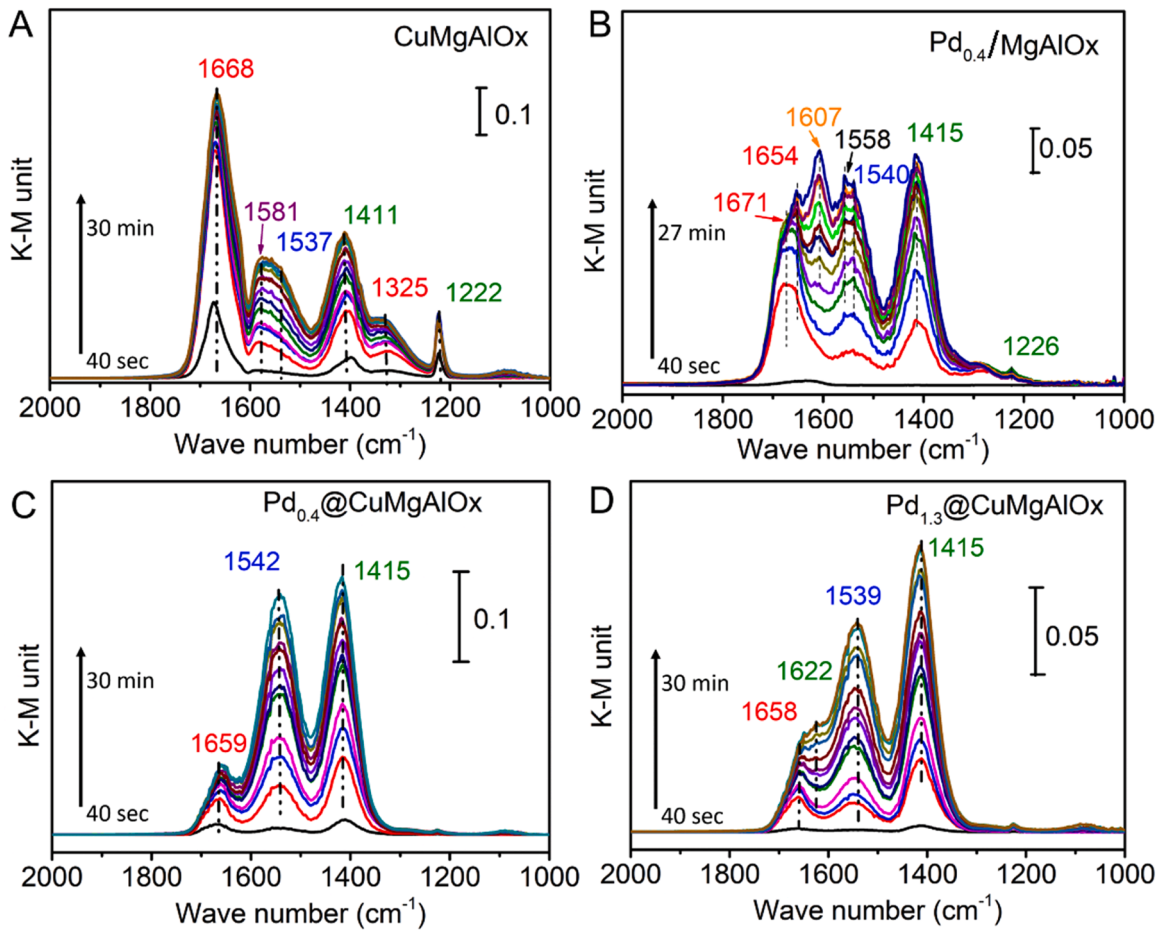

Fig. 9. *In situ* DRIFT spectra of CO_2 hydrogenation reaction under the atmosphere of CO_2 and H_2 (1:3) at 100 °C. The first three spectra were recorded every 40 s, and the rest data were collected every 3 min.

monodentate carbonate and bicarbonate. The results might be ascribed to the higher H_2-dissociation ability on the Pd-based catalysts than that on Cu-based catalysts, which promoted the hydrogenation process of the surface bidentate carbonates [25,26]. In particular, compared to the PdCu bimetallic catalysts, bidentate carbonate with higher intensity was accumulated on the $Pd_{0.4}$ @MgAlOx, indicating the insufficient H_2-dissociation ability over the monometallic Pd-based catalyst, indicating the importance of the synergetic effect on PdCu bimetallic catalysts. In this set of in situ DRIFTs experiments, $Pd_{1.3}$ @CuMgAlOx was chosen as the control sample to compare with the optimal catalyst due to its highest content of Pd but poor performance. Compared to the $Pd_{0.4}$ @CuMgAlOx catalyst, a different IR band at 1622 cm^{-1} (bicarbonate species) and a lower intensity ratio of monodentate / bicarbonate species were observed over $Pd_{1.3}$ @CuMgAlOx. It was reported that catalysts with high Pd content usually exhibited superior H_2-dissociation ability [58,59]. What's more, the hydrogen atoms can be stored by the surface and subsurface Pd atoms in the format of Pd-H hydride. Therefore, the particular bicarbonate species over $Pd_{1.3}$ @CuMgAlOx catalysts may originate from the reaction between the surface stored H species and absorbed carbonates, limiting their further conversion to the formate.

3.5. *Feasible reaction route on confined PdCu catalysts for CO_2 hydrogenation to formate*

Based on the results of $NaHCO_3$ hydrogenation experiments, it indicated that HCO_3^- was a key intermediate and gaseous CO_2 was an important supply in the CO_2 hydrogenation reaction to formate. The obtained reaction order of CO_2 and H_2 (CO_2: 0.64, H_2:1.28) further suggested that CO_2 hydrogenation over $Pd_{0.4}$ @CuMgAlOx was more dependent on the H_2 pressure. The in situ DRFTs results showed that HCO_3^-/ $HCOO^-$ were formed from the hydrogenation of absorbed bidentate carbonate and monodentate carbonate. According to the previous reported on PdAg alloy [28,52] and PdCu alloy [42] for CO_2 hydrogenation to formate, we propose a feasible reaction route for the CO_2 hydrogenation when using $Pd_{0.4}$ @CuMgAlOx catalyst. As shown in Fig. 10, in the first step, the dissociation of H_2 occurred over the metallic species, while CO_2 was absorbed on the basic sites of $Pd_{0.4}$ @CuMgAlOx catalyst forming the surface bidentate and monodentate carbonates species. In the second step, HCO_3^- was generated via the hydrogen attacking surface absorbed carbonates species. Finally, the product formate was formed via the two-step hydrogenation of HCO_3^- accompanying H_2O generation, i.e., two hydrogen atoms would attack the carbon atom and OH group simultaneously for generating H_2O and formate group, which would desorb from the catalyst surface as the hydrogenation product.

4. Conclusions

In summary, Cu confined in the MgAl-LDH structure was deleveled to stabilize Pd species for the enhanced CO_2 hydrogenation to formate. The optimal confined $Pd_{0.4}$ @CuMgAlOx catalysts displayed the highest formate formation rate of 12.8 mmol/h/g_{metal} under 100 °C, 4.0 MPa, and H_2/CO_2 ratio of 3, which was doubled the sum of the monometallic catalysts. The confined structure from the ordered hydrotalcite structure optimized metal-support interaction between PdCu species and gave the

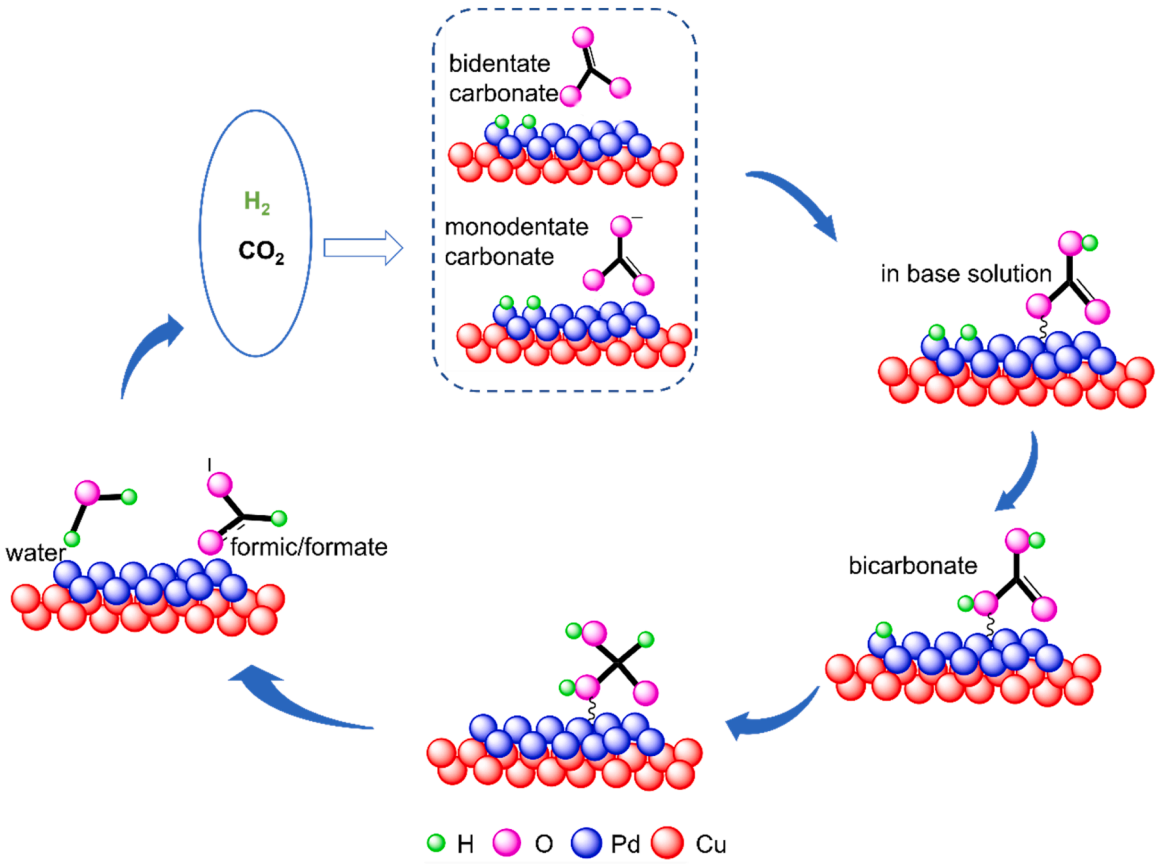

Fig. 10. Schematic representation of the plausible reaction route over confined PdCu catalysts for CO_2 hydrogenation to formate.

good catalytic stability over the $Pd_{0.4}$ @CuMgAlOx catalyst. The kinetic studies, investigation of reaction intermediate $NaHCO_3$ hydrogenation and in situ DRIFTs results supported that the formate was originated from the hydrogenation of the bidentate carbonate and monodentate carbonate species. The $Pd_{0.4}$ @CuMgAlOx sample with the electron-rich PdCu surface favored the hydrogenation of $NaHCO_3$ and further determined the catalytic activity in the hydrogenation of CO_2. This study provided a novel route for synthesizing surface-Pd rich bimetallic catalysts with confined particle sizes. Meanwhile, a well-understood confined PdCu catalysts in this contribution also showcased a promising opportunity for using LDH derived catalyst in CO_2 hydrogenation into formate.

CRediT authorship contribution statement

Xin Xiao: Conceptualization, Investigation, Writing orginal draft, Manuscript preparation. **Jiajian Gao**: In situ DRIFTs advice and results discussion, Manuscript revision, Formal analysis. **Shibo Xi**: XAS experiments, implementation and analysis, EXAFS analysis and data interpretation. **San Hua Lim:** Manuscript modification, Formal analysis, Simulation and mechanism discussion. **Alyssa Kai Wen Png**: DRIFTs experiments implementation and data collection, In situ experiment studies and interpretation, Language polishing. **Armando Borgna:** Results discussion, Funding acquisition and revision. **Wei Chu**: Supervision, Manuscript revision. **Yan Liu**: Supervision, Formal analysis, Manuscript revision, Funding acquisition.

Declaration of Competing Interest

The authors declare that they have no known competing financial interests or personal relationships that could have appeared to influence the work reported in this paper.

Acknowledgments

The authors gratefully acknowledge Dr. Kelvin Mingyao Kwok and Ms. Wang Zhan April (ICES, A*STAR, Singapore) to support the TEM and XPS tests. The authors kindly thank Mr. Andrew Lim, Joy Ng Chun Qi, and Wang Luo (ICES, A*STAR, Singapore) for supporting the TPR/TPD, SEM, and BET test. Thanks to the China Scholarship Council (CSC) for providing the Ph.D. scholarship and ICES (A-STAR, Singapore) for the financial support.

Appendix A. Supplementary material

Supplementary data associated with this article can be found in the online version at doi:10.1016/j.apcatb.2022.121239.

References

[1] G. Centi, E.A. Quadrelli, S. Perathoner, Catalysis for CO_2 conversion: a key technology for rapid introduction of renewable energy in the value chain of chemical industries, Energy Environ. Sci. 6 (2013) 1711–1731.
[2] W. Zhou, K. Cheng, J. Kang, C. Zhou, V. Subramanian, Q. Zhang, Y. Wang, New horizon in C1 chemistry: breaking the selectivity limitation in transformation of syngas and hydrogenation of CO_2 into hydrocarbon chemicals and fuels, Chem. Soc. Rev. 48 (2019) 3193–3228.
[3] X. Xiao, J. Wang, J. Li, H. Dai, F. Jing, Y. Liu, W. Chu, Enhanced low-temperature catalytic performance in CO_2 hydrogenation over Mn-promoted NiMgAl catalysts derived from quaternary hydrotalcite-like compounds, Int. J. Hydrog. Energy (2021) 33107–33119.
[4] R. Sun, Y. Liao, S.-T. Bai, M. Zheng, C. Zhou, T. Zhang, B.F. Sels, Heterogeneous catalysts for CO_2 hydrogenation to formic acid/formate: from nanoscale to single atom, Energy Environ. Sci. 14 (2021) 1247–1285.
[5] X. Su, X.F. Yang, Y. Huang, B. Liu, T. Zhang, Single-atom catalysis toward efficient CO_2 conversion to CO and formate products, Acc. Chem. Res 52 (2019) 656–664.
[6] S. Kar, A. Goeppert, G.K.S. Prakash, Integrated CO_2 capture and conversion to formate and methanol: connecting two threads, Acc. Chem. Res. 52 (2019) 2892–2903.

[7] G.H. Gunasekar, J. Shin, K.-D. Jung, K. Park, S. Yoon, Design strategy toward recyclable and highly efficient heterogeneous catalysts for the hydrogenation of CO_2 to formate, ACS Catal. 8 (2018) 4346–4353.

[8] G.H. Gunasekar, K.D. Jung, S. Yoon, Hydrogenation of CO_2 to formate using a simple, recyclable, and efficient heterogeneous catalyst, Inorg. Chem. 58 (2019) 3717–3723.

[9] X. Fu, L. Peres, J. Esvan, C. Amiens, K. Philippot, N. Yan, An air-stable, reusable Ni@Ni(OH)$_2$ nanocatalyst for CO_2/bicarbonates hydrogenation to formate, Nanoscale 13 (2021) 8931–8939.

[10] H. Wang, Y. Chi, D. Gao, Z. Wang, C. Wang, L. Wang, M. Wang, D. Cheng, J. Zhang, C. Wu, Z. Zhao, Enhancing formic acid dehydrogenation for hydrogen production with the metal/organic interface, Appl. Catal. B Environ. 255 (2019) 117776–117783.

[11] Z. Zhang, S.-W. Cao, Y. Liao, C. Xue, Selective photocatalytic decomposition of formic acid over AuPd nanoparticle-decorated TiO_2 nanofibers toward high-yield hydrogen production, Appl. Catal. B Environ. 162 (2015) 204–209.

[12] P. Liu, X. Gu, H. Zhang, J. Cheng, J. Song, H. Su, Visible-light-driven catalytic activity enhancement of Pd in AuPd nanoparticles for hydrogen evolution from formic acid at room temperature, Appl. Catal. B Environ. 204 (2017) 497–504.

[13] Y. Karatas, A. Bulut, M. Yurderi, I.E. Ertas, O. Alal, M. Gulcan, M. Celebi, H. Kivrak, M. Kaya, M. Zahmakiran, PdAu-MnO nanoparticles supported on amine-functionalized SiO_2 for the room temperature dehydrogenation of formic acid in the absence of additives, Appl. Catal. B Environ. 180 (2016) 586–595.

[14] T. Schaub, R.A. Paciello, A process for the synthesis of formic acid by CO_2 hydrogenation: thermodynamic aspects and the role of CO, Angew. Chem. Int. Ed. Engl. 50 (2011) 7278–7282.

[15] J. Fidalgo, M. Ruiz-Castaneda, G. Garcia-Herbosa, A. Carbayo, F.A. Jalon, A. M. Rodriguez, B.R. Manzano, G. Espino, Versatile Rh- and Ir-based catalysts for CO_2 hydrogenation, formic acid dehydrogenation, and transfer hydrogenation of quinolines, Inorg. Chem. 57 (2018) 14186–14198.

[16] J.B. Curley, N.E. Smith, W.H. Bernskoetter, N. Hazari, B.Q. Mercado, Catalytic formic acid dehydrogenation and CO_2 hydrogenation using iron PNRP pincer complexes with isonitrile ligands, Organometallics 37 (2018) 3846–3853.

[17] Y. Himeda, S. Miyazawa, T. Hirose, Interconversion between formic acid and H_2/CO_2 using rhodium and ruthenium catalysts for CO_2 fixation and H_2 storage, ChemSusChem 4 (2011) 487–493.

[18] C. Mondelli, B. Puertolas, M. Ackermann, Z. Chen, J. Perez-Ramirez, Enhanced base-free formic acid production from CO_2 on Pd/g-C3N4 by tuning of the carrier defects, ChemSusChem 11 (2018) 2859–2869.

[19] M.S. Maru, S. Ram, R.S. Shukla, N.-U.H. Khan, Ruthenium-hydrotalcite (Ru-HT) as an effective heterogeneous catalyst for the selective hydrogenation of CO_2 to formic acid, Mol. Catal. 446 (2018) 23–30.

[20] H. Zhong, M. Iguchi, M. Chatterjee, T. Ishizaka, M. Kitta, Q. Xu, H. Kawanami, Interconversion between CO_2 and HCOOH under basic conditions catalyzed by PdAu nanoparticles supported by amine-functionalized reduced graphene oxide as a dual catalyst, ACS Catal. 8 (2018) 5355–5362.

[21] S. Masuda, K. Mori, Y. Futamura, H. Yamashita, PdAg nanoparticles supported on functionalized mesoporous carbon: promotional effect of surface amine groups in reversible hydrogen delivery/storage mediated by formic acid/CO_2, ACS Catal. 8 (2018) 2277–2285.

[22] Q. Sun, B.W.J. Chen, N. Wang, Q. He, A. Chang, C.M. Yang, H. Asakura, T. Tanaka, M.J. Hulsey, C.H. Wang, J. Yu, N. Yan, Zeolite-encaged Pd-Mn nanocatalysts for CO_2 hydrogenation and formic acid dehydrogenation, Angew. Chem. Int. Ed. Engl. 59 (2020) 20183–20191.

[23] L.T.M. Nguyen, H. Park, M. Banu, J.Y. Kim, D.H. Youn, G. Magesh, W.Y. Kim, J. S. Lee, Catalytic CO_2 hydrogenation to formic acid over carbon nanotube-graphene supported PdNi alloy catalysts, RSC Adv. 5 (2015) 105560–105566.

[24] Z. Zhang, L. Zhang, M.J. Hülsey, N. Yan, Zirconia phase effect in Pd/ZrO_2 catalyzed CO_2 hydrogenation into formate, Mol. Catal. 475 (2019) 1–8.

[25] Z. Zhang, L. Zhang, S. Yao, X. Song, W. Huang, M.J. Hülsey, N. Yan, Support-dependent rate-determining step of CO_2 hydrogenation to formic acid on metal oxide supported Pd catalysts, J. Catal. 376 (2019) 57–67.

[26] L. Fan, J. Zhang, K. Ma, Y. Zhang, Y.-M. Hu, L. Kong, A.-P. Jia, Z. Zhang, W. Huang, J.-Q. Lu, Ceria morphology-dependent Pd-CeO_2 interaction and catalysis in CO_2 hydrogenation into formate, J. Catal. 397 (2021) 116–127.

[27] E.H. Kim, Y.H. Choi, M.H. Lee, J. Kim, H.B. Kim, K.Y. Kim, E.C. Ra, J.H. Lee, J. S. Lee, Base-free CO_2 hydrogenation to formic acid over Pd supported on defective carbon nitride modified by microwave and acid treatments, J. Catal. 396 (2021) 395–401.

[28] K. Mori, T. Sano, H. Kobayashi, H. Yamashita, Surface engineering of a supported PdAg catalyst for hydrogenation of CO_2 to formic acid: elucidating the active Pd atoms in alloy nanoparticles, J. Am. Chem. Soc. 140 (2018) 8902–8909.

[29] Z. Guo, D. Liu, S.H. Lim, Y. Liu, W. Chu, Confined PtNi catalysts for enhanced catalytic performances in one-pot cellobiose conversion to hexitols: a combined experimental and DFT study, Green Chem. 21 (2019) 5999–6011.

[30] N. Li, X. Liu, J. Zhou, Q. Ma, M. Liu, W. Chen, Enhanced Ni/W/Ti catalyst stability from Ti–O–W linkage for effective conversion of cellulose into ethylene glycol, ACS Sustain. Chem. Eng. 8 (2020) 9650–9659.

[31] W. Liu, Y. Chen, H. Qi, L. Zhang, W. Yan, X. Liu, X. Yang, S. Miao, W. Wang, C. Liu, A. Wang, J. Li, T. Zhang, A durable nickel single-atom catalyst for hydrogenation reactions and cellulose valorization under harsh conditions, Angew. Chem. Int. Ed. Engl. 57 (2018) 7071–7075.

[32] K. Yan, Y. Liu, Y. Lu, J. Chai, L. Sun, Catalytic application of layered double hydroxide-derived catalysts for the conversion of biomass-derived molecules, Catal. Sci. Technol. 7 (2017) 1622–1645.

[33] J. Fan, H. Du, Y. Zhao, Q. Wang, Y. Liu, D. Li, J. Feng, Recent progress on rational design of bimetallic Pd based catalysts and their advanced catalysis, ACS Catal. 10 (2020) 13560–13583.

[34] X. Xiao, S.H. Lim, W. Chu, Y. Liu, Chitosan-derived porous N-doped carbon as a promising support for Ru catalysts in one-pot conversion of cellobiose to hexitol, ACS Sustain. Chem. Eng. 9 (2021) 12655–12662.

[35] Y. Du, Y. Zhu, S. Xi, P. Yang, H.O. Moser, M.B.H. Breese, A. Borgna, XAFCA: a new XAFS beamline for catalysis research, J. Synchrotron Radiat. 22 (2015) 839–843.

[36] B. Li, Z. Xu, F. Jing, S. Luo, N. Wang, W. Chu, Improvement of catalytic stability for CO_2 reforming of methane by copper promoted Ni-based catalyst derived from layered-double hydroxides, J. Energy Chem. 25 (2016) 1078–1085.

[37] F. Jing, Y. Zhang, S. Luo, W. Chu, W. Qian, Nano-size MZnAl (M=Cu, Co, Ni) metal oxides obtained by combining hydrothermal synthesis with urea homogeneous precipitation procedures, Appl. Clay Sci. 48 (2010) 203–207.

[38] Y. Chen, H. Hong, J. Cai, Z. Li, Highly efficient CO_2 to CO transformation over cu-based catalyst derived from a CuMgAl-layered double hydroxide (LDH), ChemCatChem 13 (2020) 656–663.

[39] Z. Xu, N. Wang, W. Chu, J. Deng, S. Luo, In situ controllable assembly of layered-double-hydroxide-based nickel nanocatalysts for carbon dioxide reforming of methane, Catal. Sci. Technol. 5 (2015) 1588–1597.

[40] Z. Guo, J.E. Zheng, Y. Liu, W. Chu, Insight into the role of metal/oxide interaction and Ni availabilities on NiAl mixed metal oxide catalysts for methane decomposition, Appl. Catal. A Gen. 555 (2018) 1–11.

[41] X. Zhai, J. Shamoto, H. Xie, Y. Tan, Y. Han, N. Tsubaki, Study on the deactivation phenomena of Cu-based catalyst for methanol synthesis in slurry phase, Fuel 87 (2008) 430–434.

[42] G. Yang, Y. Kuwahara, K. Mori, C. Louis, H. Yamashita, Pd–Cu alloy nanoparticles confined within mesoporous hollow carbon spheres for the hydrogenation of CO_2 to formate, J. Phys. Chem. C (2021) 3961–3971.

[43] M. Wang, J. Zhang, N. Yan, Transformation of sodium bicarbonate and CO_2 into sodium formate over NiPd nanoparticle catalyst, Front. Chem. 1 (2013) 1–17.

[44] J. Chen, S. Wang, L. Peres, V. Collière, K. Philippot, P. Lecante, Y. Chen, N. Yan, Oxidation of methane to methanol over Pd@Pt nanoparticles under mild conditions in water, Catal. Sci. Technol. 11 (2021) 3493–3500.

[45] S. Zhang, C.R. Chang, Z.Q. Huang, J. Li, Z. Wu, Y. Ma, Z. Zhang, Y. Wang, Y. Qu, High catalytic activity and chemoselectivity of sub-nanometric Pd clusters on porous nanorods of CeO_2 for hydrogenation of nitroarenes, J. Am. Chem. Soc. 138 (2016) 2629–2637.

[46] P. Verma, S. Zhang, S. Song, K. Mori, Y. Kuwahara, M. Wen, H. Yamashita, T. An, Recent strategies for enhancing the catalytic activity of CO_2 hydrogenation to formate/formic acid over Pd-based catalyst, J. CO2 Util. 54 (2021) 101765–101778.

[47] H. Park, J.H. Lee, E.H. Kim, K.Y. Kim, Y.H. Choi, D.H. Youn, J.S. Lee, A highly active and stable palladium catalyst on a g-C3N4 support for direct formic acid synthesis under neutral conditions, Chem. Commun. 52 (2016) 14302–14305.

[48] R. Khobragade, P. Dahake, N. Labhsetwar, G. Saravanan, A. PdCu, nanoalloy catalyst for preferential CO oxidation in the presence of hydrogen, New J. Chem. 45 (2021) 4246–4252.

[49] K. Kishi, M. Sasanuma, The interaction of O_2 with Cu/Ni(100) and Cu/NiO/Ni (100) surfaces studied by XPS, J. Electron Spectrosc. Relat. Phenom. 48 (1989) 421–434.

[50] A.P. Jurka Batista, Djordje Mandrino, Monika Jenko, Vincent Martin, XPS and TPR examinations of g-alumina-supported Pd-Cu catalysts, Appl. Catal. A Gen. 206 (2001) 113–124.

[51] E.M. Slavinskaya, O.A. Stonkus, R.V. Gulyaev, A.S. Ivanova, V.I. Zaikovskii, P. A. Kuznetsov, A.I. Boronin, Structural and chemical states of palladium in Pd/Al_2O_3 catalysts under self-sustained oscillations in reaction of CO oxidation, Appl. Catal. A Gen. 401 (2011) 83–97.

[52] G. Yang, Y. Kuwahara, K. Mori, C. Louis, H. Yamashita, PdAg alloy nanoparticles encapsulated in N-doped microporous hollow carbon spheres for hydrogenation of CO_2 to formate, Appl. Catal. B Environ. 283 (2021) 1–13.

[53] Y. Kuwahara, Y. Fujie, T. Mihogi, H. Yamashita, Hollow mesoporous organosilica spheres encapsulating PdAg nanoparticles and poly(ethyleneimine) as reusable catalysts for CO_2 hydrogenation to formate, ACS Catalysis 10 (2020) 6356–6366.

[54] G. Yang, Y. Kuwahara, S. Masuda, K. Mori, C. Louis, H. Yamashita, PdAg nanoparticles and aminopolymer confined within mesoporous hollow carbon spheres as an efficient catalyst for hydrogenation of CO_2 to formate, J. Mater. Chem. A 8 (2020) 4437–4446.

[55] D. Cornu, H. Guesmi, J.-M. Krafft, H. Lauron-Pernot, Lewis acido-basic interactions between CO_2 and MgO surface: DFT and DRIFT approaches, J. Phys. Chem. C 116 (2012) 6645–6654.

[56] J. Zhang, W. Liao, H. Zheng, Y. Zhang, L. Xia, B.-T. Teng, J.-Q. Lu, W. Huang, Z. Zhang, Morphology-engineered highly active and stable Pd/TiO_2 catalysts for CO_2 hydrogenation into formate, J. Catal. 405 (2022) 152–163.

[57] J. Zhang, L. Fan, F. Zhao, Y. Fu, J.Q. Lu, Z. Zhang, B. Teng, W. Huang, Zinc oxide morphology-dependent Pd/ZnO catalysis in base-free CO_2 hydrogenation into formic acid, ChemCatChem 12 (2020) 5540–5547.

[58] L. Jiang, K. Liu, S.F. Hung, L. Zhou, R. Qin, Q. Zhang, P. Liu, L. Gu, H.M. Chen, G. Fu, N. Zheng, Facet engineering accelerates spillover hydrogenation on highly diluted metal nanocatalysts, Nat. Nanotechnol. 15 (2020) 848–853.

[59] H. Dai, X. Xiao, L. Huang, C. Zhou, J. Deng, Different catalytic behavior of Pd/palygorskite catalysts for semi-hydrogenation of acetylene, Appl. Clay Sci. 211 (2021) 1–7.